

PARAMETER-FREE IMPLEMENTATION OF THE QUADRATIC C⁰ INTERIOR PENALTY METHOD FOR THE BIHARMONIC EQUATION*

PHILIPP BRINGMANN[†], CARSTEN CARSTENSEN[†], AND JULIAN STREITBERGER[‡]

Abstract. The symmetric C⁰ interior penalty method is one of the most popular discontinuous Galerkin methods for the biharmonic equation. This paper introduces an automatic selection of the involved stability parameter in terms of the geometry of the underlying triangulation. It avoids any extra input variables and guarantees a stable discretization with stability 1/2. The practical realization of this parameter-free scheme in less than 120 lines of MATLAB is described and explained in detail. Numerical experiments show stability constants smaller than 1 and so over-stabilization is excluded. The approach is documented for the lowest-order scheme in 2D for triangles, but the methodology behind can be generalized for automatic local parameter decisions.

Key words. C⁰ interior penalty method, discontinuous Galerkin method, biharmonic equation, implementation, parameter-free

AMS subject classifications. 65N12, 65N15, 65N30, 65N50, 65Y20

1. Introduction. Let $\Omega \subset \mathbb{R}^2$ be a bounded Lipschitz domain with polygonal boundary $\partial\Omega$. For a given source term $f \in L^2(\Omega)$, suppose $u \in V := H_0^2(\Omega)$ solves the biharmonic equation $\Delta^2 u = f$. The weak formulation seeks $u \in V$ with

$$(1.1) \quad a(u, v) := \int_{\Omega} \mathbb{D}^2 u : \mathbb{D}^2 v \, dx = \int_{\Omega} f v \, dx \quad \text{for all } v \in V.$$

The Riesz representation theorem applies in the Hilbert space (V, a) and proves well-posedness of the formulation (1.1). Elliptic regularity theory verifies that $f \in L^2(\Omega)$ implies $u \in H^{2+\alpha}(\Omega) \cap H_0^2(\Omega)$ [1, 5, 19, 21]. The pure Dirichlet boundary conditions in the model example lead to $\alpha > 1/2$ and allow for a control of the traces $\mathbb{D}^2 u$ in the jump terms. The conforming finite element method for the plate problem originates from the work of Argyris [2] with a quintic polynomial ansatz space $P_5(T)$ and 21 degrees of freedom on each triangle T . The practical application is less prominent due to the higher computational efforts, while classical nonconforming FEMs [11, 13, 14, 18] and discontinuous Galerkin schemes [3, 10, 11, 16, 24] appear more popular in the literature. Discontinuous Galerkin methods allow for discontinuities across triangle interfaces leading to more flexible schemes compared to their classical nonconforming pendants.

The key idea of discontinuous Galerkin methods is the replacement of the space V in the weak formulation (1.1) by the piecewise Sobolev space

$$(1.2) \quad H^2(\mathcal{T}) := \{v \in L^2(\Omega) : \forall T \in \mathcal{T}, v|_T \in H^2(T) := H^2(\text{int}(T))\}$$

with respect to a shape-regular triangulation \mathcal{T} of the domain Ω into closed triangles. For $v \in H^2(\mathcal{T})$, the piecewise application of the distributional derivatives leads to the Hessian $\mathbb{D}_{\text{pw}}^2 v \in L^2(\Omega; \mathbb{S})$, $(\mathbb{D}_{\text{pw}}^2 v)|_T := \mathbb{D}^2(v|_T)$ with values in the space $\mathbb{S} \subset \mathbb{R}^{2 \times 2}$ of symmetric 2-by-2 matrices.

*Draft from September 13, 2022.

[†]Department of Mathematics, Humboldt-Universität zu Berlin, Germany (bringman@math.hu-berlin.de, cc@math.hu-berlin.de).

[‡]Institute for Analysis and Scientific Computing, TU Wien, Austria (julian.streitberger@asc.tuwien.ac.at).

The piecewise Sobolev functions $v \in H^2(\mathcal{T})$, allow for the evaluation of averages $\langle v \rangle_E$ and jumps $[v]_E$ across an edge $E \in \mathcal{E}$. Each interior edge $E \in \mathcal{E}(\Omega)$ of length $h_E := |E|$ is the common edge of exactly two triangles $T_+, T_- \in \mathcal{T}$, written $E = \partial T_+ \cap \partial T_-$. Then

$$(1.3) \quad [v]_E := (v|_{T_+})|_E - (v|_{T_-})|_E \quad \text{and} \quad \langle v \rangle_E := \frac{1}{2}(v|_{T_+})|_E + \frac{1}{2}(v|_{T_-})|_E.$$

The unit normal vector ν_E is oriented such that $\nu_E \cdot \nu_{T_\pm}|_E = \pm 1$ for the outward unit normal vectors ν_{T_\pm} of T_\pm . For each boundary edge $E \in \mathcal{E}(\partial\Omega)$, let $T_+ \in \mathcal{T}$ denote the unique triangle with edge $E \in \mathcal{E}(T_+)$ and set $[v]_E := \langle v \rangle_E := (v|_{T_+})|_E$. Analogous definitions apply for vector- or matrix-valued polynomials. For further details on the notation, the reader is referred to the following Section 2.

The symmetric C^0 interior penalty method seeks a function $u_{\text{IP}} \in V_h := S_0^2(\mathcal{T}) := P_2(\mathcal{T}) \cap H_0^1(\Omega)$ in the quadratic Lagrange finite element space with

$$(1.4) \quad A_h(u_{\text{IP}}, v_{\text{IP}}) = \int_{\Omega} f v_{\text{IP}} \, dx \quad \text{for all } v_{\text{IP}} \in V_h.$$

The three contributions to the bilinear form $A_h : V_h \times V_h \rightarrow \mathbb{R}$,

$$(1.5) \quad A_h(u_{\text{IP}}, v_{\text{IP}}) := a_{\text{pw}}(u_{\text{IP}}, v_{\text{IP}}) - (\mathcal{J}(u_{\text{IP}}, v_{\text{IP}}) + \mathcal{J}(v_{\text{IP}}, u_{\text{IP}})) + c_{\text{IP}}(u_{\text{IP}}, v_{\text{IP}})$$

for all $u_{\text{IP}}, v_{\text{IP}} \in V_h$ originate from the triangle-wise application of the integration by parts in the derivation of the weak formulation (1.1) [10]. This leads to a piecewise version of the energy scalar product $a_{\text{pw}} : V_h \times V_h \rightarrow \mathbb{R}$ and a jump term $\mathcal{J} : V_h \times V_h \rightarrow \mathbb{R}$,

$$(1.6) \quad \begin{aligned} a_{\text{pw}}(u_{\text{IP}}, v_{\text{IP}}) &:= \sum_{T \in \mathcal{T}} \int_T \mathbf{D}^2 u_{\text{IP}} : \mathbf{D}^2 v_{\text{IP}} \, dx, \\ \mathcal{J}(u_{\text{IP}}, v_{\text{IP}}) &:= \sum_{E \in \mathcal{E}} \int_E \langle \mathbf{D}_{\text{pw}}^2 u_{\text{IP}} \nu_E \rangle_E \cdot [\nabla v_{\text{IP}}]_E \, dx \end{aligned}$$

for all $u_{\text{IP}}, v_{\text{IP}} \in V_h$. The H^2 conformity is imposed weakly by the additional penalty term $c_{\text{IP}} : V_h \times V_h \rightarrow \mathbb{R}$,

$$(1.7) \quad c_{\text{IP}}(u_{\text{IP}}, v_{\text{IP}}) := \sum_{E \in \mathcal{E}} \frac{\sigma_{\text{IP},E}}{h_E} \int_E [\nabla u_{\text{IP}} \cdot \nu_E]_E [\nabla v_{\text{IP}} \cdot \nu_E]_E \, ds \quad \text{for all } u_{\text{IP}}, v_{\text{IP}} \in V_h,$$

with some edge-dependent parameter $\sigma_{\text{IP},E} > 0$ for each $E \in \mathcal{E}$.

While the boundedness of A_h follows from standard arguments, its coercivity is typically subject to the assumption of a sufficiently large penalty parameter $\sigma_{\text{IP},E}$ [10, 12]. The contribution of this paper is twofold. First, a novel stability analysis introduces an automated mesh-dependent selection of $\sigma_{\text{IP},E}$ with some $a > 1$ by

$$(1.8) \quad \sigma_{\text{IP},E} := \begin{cases} \frac{3ah_E^2}{4} \left(\frac{1}{|T_+|} + \frac{1}{|T_-|} \right) & \text{if } E = \partial T_+ \cap \partial T_- \in \mathcal{E}(\Omega), \\ \frac{3ah_E^2}{|T_+|} & \text{if } E \in \mathcal{E}(T_+) \cap \mathcal{E}(\partial\Omega). \end{cases}$$

Every choice of $a > 1$ leads to guaranteed stability in the main result Theorem 3.1 in Section 3 below.

Second, the numerical realization of the C⁰ interior penalty method is provided in great detail. The implementation bases on the evaluation of derivatives of discrete functions $v_h \in V_h$ presented in Section 4 below. The Sections 5–7 cover the computation of the local contributions to the bilinear forms a_{pw} , \mathcal{J} , and c_{IP} from (1.6)–(1.7) and Section 8 describes the assembling of the linear system of equations. Particular focus is put on the procedure for evaluating the jumps $[\nabla v_h \cdot \nu_E]_E$ and the averages $\langle D_{pw}^2 v_h \nu_E \rangle_E$ in \mathcal{J} and c_{IP} in Section 6 below. The automatic computation of the penalty parameter $\sigma_{IP,E}$ solely requires four lines of MATLAB and avoids any manual selection by the user. The presentation aims to be easily accessible and serves as a documentation of the complete implementation given in the Appendix A.

Numerical experiments with the implementation at hand investigate the stability of the scheme with the suggested automatic penalty selection in Section 9. The coercivity constants are computed numerically and compared with the theoretically established value. Moreover, the performance of an adaptive mesh-refinement algorithm is examined. The appendix includes the complete implementation as well as a realization of an a posteriori error estimator.

2. Notation. Standard notation of Lebesgue and Sobolev spaces, their norms, and L^2 scalar products applies throughout the paper. Let \mathcal{T} denote a shape regular triangulation of the polygonal Lipschitz domain Ω into closed triangles and \mathcal{V} (resp. $\mathcal{V}(\Omega)$ or $\mathcal{V}(\partial\Omega)$) the set of all (resp. interior or boundary) vertices [7, 9]. Let \mathcal{E} (resp. $\mathcal{E}(\Omega)$ or $\mathcal{E}(\partial\Omega)$) be the set of all (resp. interior or boundary) edges. For each triangle $T \in \mathcal{T}$ of area $|T|$, let $\mathcal{V}(T)$ denote the set of its three vertices and $\mathcal{E}(T)$ the set of its three edges. Abbreviate the edge patch by $\omega_E := \text{int}(T_+ \cup T_-) \subseteq \Omega$ for an interior edge $E = \partial T_+ \cap \partial T_- \in \mathcal{E}(\Omega)$ and by $\omega_E := \text{int}(T_+) \subseteq \Omega$ for a boundary edge $E \in \mathcal{E}(T_+) \cap \mathcal{E}(\partial\Omega)$.

Define the space of piecewise polynomials

$$P_k(\mathcal{T}) := \{v \in L^2(\Omega) : v|_T \in P_k(T) \text{ for all } T \in \mathcal{T}\}$$

of total degree at most $k \in \mathbb{N}_0$.

The notation $A \lesssim B$ abbreviates $A \leq CB$ for a positive, generic constant C , solely depending on the domain Ω , the polynomial degree, and the shape regularity of the triangulation \mathcal{T} ; $A \approx B$ abbreviates $A \lesssim B \lesssim A$.

For two indices $j, k \in \mathbb{N}$, let $\delta_{jk} \in \{0, 1\}$ denote the Kronecker symbol defined by $\delta_{jk} := 1$ if and only if $j = k$. The enclosing single bars $|\bullet|$ apply context-sensitively and denote not only the modulus of real numbers, the Euclidian norm of vectors in \mathbb{R}^2 , but also the cardinality of finite sets, the area of two-dimensional Lebesgue sets, and the length of edges.

3. Stability. This section develops a *novel* stability analysis with a penalty parameter $\sigma_{IP,E}$ in the bilinear form c_{IP} from (1.7). Let the discrete space V_h be equipped with the mesh-dependent norm $\|\bullet\|_h$ defined, for $v_{IP} \in V_h$, by

$$\|v_{IP}\|_h^2 := \|v_{IP}\|_{pw}^2 + c_{IP}(v_{IP}, v_{IP}).$$

with the piecewise semi-norm $\|\bullet\|_{pw} := |\bullet|_{H^2(\mathcal{T})} := \|D_{pw}^2 \bullet\|_{L^2(\Omega)}$. The parameter $\sigma_{IP,E}$ from (1.8) solely depends on the underlying triangulation and allows for a guaranteed stability of the bilinear form A_h from (1.5) with respect to the mesh-dependent norm $\|\bullet\|_h$ in the following theorem.

THEOREM 3.1. *Given any $a > 1$, define the penalty parameter $\sigma_{IP,E} > 0$ as in (1.8). For every choice of $a > 1$, the constant $\kappa := 1 - 1/\sqrt{a} > 0$ and all discrete*

functions $v_{\text{IP}} \in V_h$ satisfy the stability estimate

$$(3.1) \quad A_h(v_{\text{IP}}, v_{\text{IP}}) \geq \kappa \|v_{\text{IP}}\|_h^2.$$

Two remarks are in order before the proof of the Theorem 3.1 concludes this section.

Remark 3.2. The penalty parameter $\sigma_{\text{IP},E}$ in (1.8) contains a prefactor $a > 1$. The striking point of Theorem 3.1 is that *every* choice of $a > 1$ leads to guaranteed stability. In the case of very large $a \rightarrow \infty$, i.e., $\sigma_{\text{IP},E} \rightarrow \infty$, the stability constant κ tends to 1. Hence, the theoretical stability constant can be improved by a large penalization. This is of particular interest, because optimal convergence rates of the adaptive discontinuous Galerkin method in [6] rely on a sufficiently large penalty parameter.

Remark 3.3. Although the presentation restricts to the quadratic case, the concept can be generalized for guaranteed stability in the case of polynomial degree $k \geq 3$. Even the assumption of uniform polynomial degree can be weakened, allowing for a different polynomial degree k_T on every triangle $T \in \mathcal{T}$.

Proof of Theorem 3.1. The point of departure is the difference, for every $\kappa > 0$,

$$(3.2) \quad \begin{aligned} A_h(v_{\text{IP}}, v_{\text{IP}}) - \kappa \|v_{\text{IP}}\|_h^2 &= (1 - \kappa) \|v_{\text{IP}}\|_{\text{pw}}^2 - 2\mathcal{J}(v_{\text{IP}}, v_{\text{IP}}) \\ &\quad + (1 - \kappa) \sum_{E \in \mathcal{E}} \frac{\sigma_{\text{IP},E}}{h_E} \|[\nabla v_{\text{IP}} \cdot \nu_E]_E\|_{L^2(E)}^2. \end{aligned}$$

The first step of the proof bounds the jump term \mathcal{J} with the weighted Young inequality, for every $\varepsilon > 0$,

$$2|\mathcal{J}(v_{\text{IP}}, v_{\text{IP}})| \leq \sum_{E \in \mathcal{E}} \left(\frac{\varepsilon \sigma_{\text{IP},E}}{h_E} \|[\nabla v_{\text{IP}}]_E\|_{L^2(E)}^2 + \frac{h_E}{\varepsilon \sigma_{\text{IP},E}} \|\langle D_{\text{pw}}^2 v_{\text{IP}} \nu_E \rangle_E\|_{L^2(E)}^2 \right).$$

Inserting this estimate into (3.2) confirms the lower bound

$$(3.3) \quad \begin{aligned} &A_h(v_{\text{IP}}, v_{\text{IP}}) - \kappa \|v_{\text{IP}}\|_h^2 \\ &\geq (1 - \kappa) \|v_{\text{IP}}\|_{\text{pw}}^2 + (1 - \kappa) \sum_{E \in \mathcal{E}} \frac{\sigma_{\text{IP},E}}{h_E} \|[\nabla v_{\text{IP}} \cdot \nu_E]_E\|_{L^2(E)}^2 \\ &\quad - \sum_{E \in \mathcal{E}} \left(\frac{\varepsilon \sigma_{\text{IP},E}}{h_E} \|[\nabla v_{\text{IP}}]_E\|_{L^2(E)}^2 + \frac{h_E}{\varepsilon \sigma_{\text{IP},E}} \|\langle D_{\text{pw}}^2 v_{\text{IP}} \nu_E \rangle_E\|_{L^2(E)}^2 \right). \end{aligned}$$

The second step estimates the average $\langle D_{\text{pw}}^2 v_{\text{IP}} \nu_E \rangle_E$. Since the piecewise second derivative $D_{\text{pw}}^2 v_{\text{IP}}$ of any function $v_{\text{IP}} \in V_h$ is constant on each triangle T , it holds that

$$(3.4) \quad \|D_{\text{pw}}^2 v_{\text{IP}}|_T\|_{L^2(E)}^2 = \frac{h_E}{|T|} \|D_{\text{pw}}^2 v_{\text{IP}}\|_{L^2(T)}^2.$$

For an interior edge $E = \partial T_+ \cap \partial T_- \in \mathcal{E}(\Omega)$ with the neighboring triangles T_+ and T_- , the definition of the average from (1.3) and $|\nu_E| = 1$ verify

$$\|\langle D_{\text{pw}}^2 v_{\text{IP}} \nu_E \rangle_E\|_{L^2(E)}^2 \leq \frac{1}{4} \|D^2 v_{\text{IP}}|_{T_+} + D^2 v_{\text{IP}}|_{T_-}\|_{L^2(E)}^2.$$

The combination with a triangle inequality, another weighted Young inequality with $\alpha > 0$, and (3.4) results in

$$\|\langle D_{\text{pw}}^2 v_{\text{IP}} \nu_E \rangle_E\|_{L^2(E)}^2 \leq \frac{h_E}{4} \left(\frac{1 + \alpha}{|T_+|} \|D^2 v_{\text{IP}}\|_{L^2(T_+)}^2 + \frac{1 + 1/\alpha}{|T_-|} \|D^2 v_{\text{IP}}\|_{L^2(T_-)}^2 \right).$$

Hence the optimal value $\alpha = |T_+|/|T_-|$ leads to

$$\|\langle D_{\text{pw}}^2 v_{\text{IP}} \nu_E \rangle_E\|_{L^2(E)}^2 \leq \frac{h_E}{4} \left(\frac{1}{|T_+|} + \frac{1}{|T_-|} \right) \|D_{\text{pw}}^2 v_{\text{IP}}\|_{L^2(\omega_E)}^2.$$

The multiplication with $h_E/(\varepsilon\sigma_{\text{IP},E})$ and the definition of $\sigma_{\text{IP},E}$ in (1.8) show

$$(3.5) \quad \frac{h_E}{\varepsilon\sigma_{\text{IP},E}} \|\langle D_{\text{pw}}^2 v_{\text{IP}} \nu_E \rangle_E\|_{L^2(E)}^2 \leq \frac{1}{3a\varepsilon} \|D_{\text{pw}}^2 v_{\text{IP}}\|_{L^2(\omega_E)}^2.$$

For a boundary edge $E \in \mathcal{E}(\partial\Omega)$ with adjacent triangle $T_+ \in \mathcal{T}$, the definition of the average, the equality $|\nu_E| = 1$, and (3.4) verify

$$\|\langle D_{\text{pw}}^2 v_{\text{IP}} \nu_E \rangle_E\|_{L^2(E)}^2 = \|D_{\text{pw}}^2 v_{\text{IP}} \nu_E\|_{L^2(E)}^2 \leq \|D_{\text{pw}}^2 v_{\text{IP}}\|_{L^2(E)}^2 = \frac{h_E}{|T_+|} \|D^2 v_{\text{IP}}\|_{L^2(T_+)}^2.$$

Consequently, the multiplication with $h_E/(\varepsilon\sigma_{\text{IP},E})$ and the definition of the penalty parameter $\sigma_{\text{IP},E}$ result in the analogous estimate (3.5) for $E \in \mathcal{E}(\partial\Omega)$.

The sum of (3.5) over all edges $E \in \mathcal{E}$ and the finite overlap of the edge patches $(\omega(E) : E \in \mathcal{E})$ lead to

$$(3.6) \quad \sum_{E \in \mathcal{E}} \frac{h_E}{\varepsilon\sigma_{\text{IP},E}} \|\langle D_{\text{pw}}^2 v_{\text{IP}} \nu_E \rangle_E\|_{L^2(E)}^2 \leq \frac{1}{a\varepsilon} \|v_{\text{IP}}\|_{\text{pw}}^2.$$

The third step investigates the jump $[\nabla v_{\text{IP}}]_E$. The analysis of the jump term employs the orthogonal split into the tangential and normal component [15, Section 6]. On each edge $E \in \mathcal{E}$, the jump $[\nabla v_{\text{IP}}]_E$ fulfills

$$[\nabla v_{\text{IP}}]_E = ([\nabla v_{\text{IP}}]_E \cdot \tau_E) \tau_E + ([\nabla v_{\text{IP}}]_E \cdot \nu_E) \nu_E.$$

For any interior edge $E = \partial T_+ \cap \partial T_- \in \mathcal{E}(\Omega)$ with the adjacent triangles T_+ and T_- , the function v_{IP} is differentiable in T_+ and T_- . The Hadamard jump condition for the globally continuous function v_{IP} assures that the tangential derivatives from the adjacent triangles coincide [4, p. 30]. This means that the term $[\nabla v_{\text{IP}}]_E \cdot \tau_E$ vanishes and

$$(3.7) \quad [\nabla v_{\text{IP}}]_E = ([\nabla v_{\text{IP}}]_E \cdot \nu_E) \nu_E.$$

For any boundary edge $E \in \mathcal{E}(\partial\Omega)$, the homogeneous boundary values of the function $v_{\text{IP}} \in V_h$ guarantee that the tangential derivative vanishes. This and the jump with zero in the definition (1.3) show

$$[\nabla v_{\text{IP}}]_E = \nabla(v_{\text{IP}}|_{T_+})|_E = (\nabla(v_{\text{IP}}|_{T_+})|_E \cdot \nu_E) \nu_E = ([\nabla v_{\text{IP}}]_E \cdot \nu_E) \nu_E.$$

Hence, for all $E \in \mathcal{E}$,

$$(3.8) \quad \|[\nabla v_{\text{IP}}]_E\|_{L^2(E)}^2 = \|[\nabla v_{\text{IP}}]_E \cdot \nu_E\|_{L^2(E)}^2.$$

The fourth step concludes the proof with a combination of the lower bound (3.3), the estimate (3.6), and the identity (3.8) for

$$(3.9) \quad \begin{aligned} A_h(v_{\text{IP}}, v_{\text{IP}}) - \kappa \|v_{\text{IP}}\|_h^2 &\geq \left(1 - \kappa - \frac{1}{a\varepsilon}\right) \|v_{\text{IP}}\|_{\text{pw}}^2 \\ &\quad + (1 - \kappa - \varepsilon) \sum_{E \in \mathcal{E}} \frac{\sigma_{\text{IP},E}}{h_E} \|[\nabla v_{\text{IP}}]_E \cdot \nu_E\|_{L^2(E)}^2. \end{aligned}$$

Every choice of $0 < \kappa \leq \min\{1 - 1/(a\varepsilon), 1 - \varepsilon\}$ leads to a nonnegative lower bound in (3.9), and proves the claim (3.1). The optimal value $\varepsilon = 1/\sqrt{a}$ allows for $\kappa = 1 - 1/\sqrt{a}$. \square

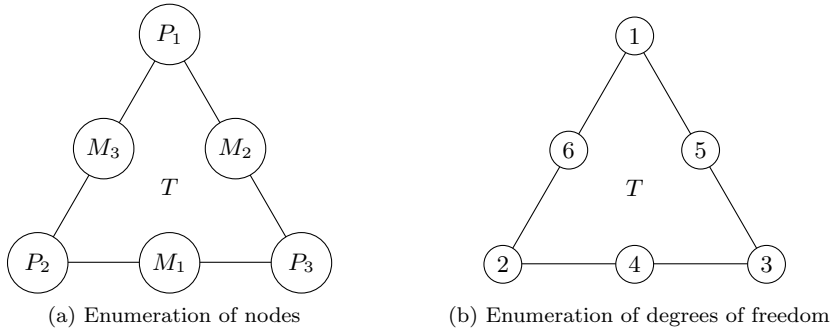


FIG. 1. Local enumeration of nodes associated to the piecewise quadratic basis functions in the triangle T .

4. Discrete functions and their derivatives. The presentation of the MATLAB realization of the C^0 interior penalty method departs with the definition of the quadratic shape functions. This section illustrates the evaluation of their derivatives of first and second order and provides the foundation for the computation of the local contributions to the bilinear forms in A_h in the Sections 5–7 below.

Two key data structures represent the underlying triangulation \mathcal{T} . The rows of the array $\mathbf{c4n} \in \mathbb{R}^{|\mathcal{V}| \times 2}$ contain the two coordinates of each vertex in \mathcal{V} . The order of the vertices in the array determines their enumeration. Three vertices form a triangle and their numbers are stored in the rows of the array $\mathbf{n4e} \in \mathbb{N}^{|\mathcal{T}| \times 3}$ in counter-clockwise order.

Let $T \in \mathcal{T}$ denote a triangle of global number $\mathbf{e} \in \{1, \dots, |\mathcal{T}|\}$, i.e., the global indices of its three vertices $\mathcal{V}(T) = \{P_1, P_2, P_3\}$ belong to the \mathbf{e} -th row of $\mathbf{c4n}$. The enumeration of the midpoints M_1, M_2, M_3 of the three edges $\mathcal{E}(T) = \{E_1, E_2, E_3\}$ follows the convention that the edge E_j is opposite to the node P_j for $j = 1, 2, 3$ as depicted in Figure 1a. Let $\lambda_j \in P_1(T)$ denote the barycentric coordinate associated to the vertex P_j of the triangle T for $j = 1, 2, 3$. Since $x = \lambda_1(x)P_1 + \lambda_2(x)P_2 + \lambda_3(x)P_3$ and $1 = \lambda_1(x) + \lambda_2(x) + \lambda_3(x)$ for all $x \in T$, the gradients $\nabla\lambda_1, \nabla\lambda_2, \nabla\lambda_3$ are determined by the linear system of equations

$$(4.1) \quad \begin{bmatrix} 1 & 1 & 1 \\ P_1 & P_2 & P_3 \end{bmatrix} \begin{bmatrix} \nabla\lambda_1^\top \\ \nabla\lambda_2^\top \\ \nabla\lambda_3^\top \end{bmatrix} = \begin{bmatrix} 0 & 0 \\ 1 & 0 \\ 0 & 1 \end{bmatrix}.$$

LEMMA 4.1. *Let the three-dimensional array $\mathbf{c4e} \in \mathbb{R}^{2 \times 3 \times |\mathcal{T}|}$ contain the matrix $[P_1 \ P_2 \ P_3] \in \mathbb{R}^{2 \times 3}$ for each triangle $T \in \mathcal{T}$. The following line of MATLAB computes the gradients $\nabla\lambda_1, \nabla\lambda_2, \nabla\lambda_3$, according to (4.1).*

```
GradP1 = [ones(1,3); c4e(:, :, e)] \ [zeros(1,2); eye(2)];
```

Proof. The backslash operator in MATLAB calls the function `mldivide` and solves the linear system (4.1) up to machine precision. The three rows of the solution array $\mathbf{GradP1} \in \mathbb{R}^{3 \times 2}$ contain the two components of the constant gradients. \square

The shape functions ϕ_1, \dots, ϕ_6 of $P_2(T)$ can be represented using products of the barycentric coordinates. Throughout this section, let $\{j, k, \ell\} = \{1, 2, 3\}$ denote any pairwise distinct indices. The quadratic shape function $\phi_j := \lambda_j(2\lambda_j - 1)$ is associated

to the vertex P_j and $\phi_{3+j} := 4\lambda_k\lambda_\ell$ to the midpoint M_j of E_j . They satisfy the duality

$$\phi_j(P_n) = \delta_{jn} = \phi_{3+j}(M_n) \quad \text{and} \quad \phi_j(M_n) = 0 = \phi_{3+j}(P_n) \quad \text{for all } j, n = 1, 2, 3.$$

The enumeration of ϕ_1, \dots, ϕ_6 is illustrated in Figure 1b. The representation via barycentric coordinates and the product rule lead to the following formulas for the derivatives of first and second order. For pairwise distinct indices $\{j, k, \ell\} = \{1, 2, 3\}$,

$$(4.2) \quad \nabla\phi_j = (4\lambda_j - 1)\nabla\lambda_j, \quad \nabla\phi_{3+j} = 4(\lambda_k\nabla\lambda_\ell + \lambda_\ell\nabla\lambda_k),$$

$$(4.3) \quad D^2\phi_j = 4\nabla\lambda_j \otimes \nabla\lambda_j, \quad D^2\phi_{3+j} = 4(\nabla\lambda_k \otimes \nabla\lambda_\ell + \nabla\lambda_\ell \otimes \nabla\lambda_k).$$

Hence, the evaluation of the gradients $\nabla\phi_1, \dots, \nabla\phi_6$ in the three nodes P_k , M_j , and P_ℓ reads, for pairwise distinct indices $\{j, k, \ell\} = \{1, 2, 3\}$,

$$(4.4) \quad \begin{bmatrix} \nabla\phi_j(P_j) & \nabla\phi_j(P_k) \\ \nabla\phi_j(M_j) & \nabla\phi_j(M_k) \\ \nabla\phi_{3+j}(P_j) & \nabla\phi_{3+j}(P_k) \\ \nabla\phi_{3+j}(M_j) & \nabla\phi_{3+j}(M_k) \end{bmatrix} = \begin{bmatrix} 3\nabla\lambda_j & -\nabla\lambda_j \\ -\nabla\lambda_j & \nabla\lambda_j \\ 0 & 4\nabla\lambda_\ell \\ 2(\nabla\lambda_k + \nabla\lambda_\ell) & 2\nabla\lambda_k \end{bmatrix}.$$

LEMMA 4.2. *The following lines of MATLAB realize the evaluation of the gradients from (4.4).*

```
Gradient = cat(3, [3 -1 -1 -1 1 1] .* GradP1(1,:)', ...
                 [-1 3 -1 1 -1 1] .* GradP1(2,:)', ...
                 [-1 -1 3 1 1 -1] .* GradP1(3,:)', ...
                 [0 0 4 2 2 0] .* GradP1(2,:)', ...
                 + [0 4 0 2 0 2] .* GradP1(3,:)', ...
                 [0 0 4 2 2 0] .* GradP1(1,:)', ...
                 + [4 0 0 0 2 2] .* GradP1(3,:)', ...
                 [0 4 0 2 0 2] .* GradP1(1,:)', ...
                 + [4 0 0 0 2 2] .* GradP1(2,:)');
```

Proof. Linear combinations of the gradients of the barycentric coordinates from GradP1 provide the formulas in (4.4). They are rearranged and stored in the three-dimensional array Gradient $\in \mathbb{R}^{2 \times 6 \times 6}$. \square

LEMMA 4.3. *The following lines of MATLAB evaluate the piecewise constant Hessian matrices from (4.3).*

```
H = permute(GradP1, [2 3 1 4]) .* permute(GradP1, [3 2 4 1]);
Hessian = 4 * cat(3, H(:, :, 1, 1), H(:, :, 2, 2), H(:, :, 3, 3), ...
                  H(:, :, 2, 3) + H(:, :, 3, 2), ...
                  H(:, :, 1, 3) + H(:, :, 3, 1), ...
                  H(:, :, 1, 2) + H(:, :, 2, 1));
```

Proof. All pairwise tensor products of the gradients of the barycentric coordinates from Lemma 4.1 result in nine 2-by-2 matrices. They are stored in the four-dimensional array H $\in \mathbb{R}^{2 \times 2 \times 3 \times 3}$. The linear combinations of these matrices provide the Hessian matrices $D^2\phi_1, \dots, D^2\phi_6$ in the array Hessian $\in \mathbb{R}^{2 \times 2 \times 6}$. \square

Remark 4.4. The Hessian matrices Hessian $\in \mathbb{R}^{2 \times 2 \times 6}$ from Lemma 4.3 and the gradient evaluations Gradient $\in \mathbb{R}^{2 \times 6 \times 6}$ are computed elementwise and stored in the global variables Hess4e $\in \mathbb{R}^{6 \times 2 \times 2 \times |\mathcal{T}|}$ and Grad4e $\in \mathbb{R}^{6 \times 2 \times 6 \times |\mathcal{T}|}$ by

```
Hess4e(:, :, :, e) = permute(Hessian, [3 1 2]);
Grad4e(:, :, :, e) = permute(Gradient, [3 1 2]);
```

The evaluations of the derivatives are supposed to be used in a parallelized computation over all edges for the local contributions in the Sections 6–7 below. In order to comply with the requirements of MATLAB’s parallel toolbox, the data structures are rearranged in an edge-oriented way

$$\mathbf{Hess4s} \in \mathbb{R}^{6 \times 2 \times 2 \times 2 \times |\mathcal{E}|} \quad \text{and} \quad \mathbf{Grad4s} \in \mathbb{R}^{6 \times 2 \times 6 \times 2 \times |\mathcal{E}|}.$$

For each edge, they contain the corresponding information on the adjacent triangles $T_+, T_- \in \mathcal{T}$ specified by the index in the fourth component (index 1 for T_+ and 2 for T_-). The rearrangement employs a data structure $\mathbf{e4s}$ whose rows contain the global indices of T_+ and T_- for interior edges or the global index of T_+ and 0 for boundary edges. For the realization, see the lines 70–75 of the program in Appendix A.

5. Stiffness matrix and right-hand side. The contribution to the bilinear form a_{pw} from the triangle $T \in \mathcal{T}$ leads to the local stiffness matrix $A(T) \in \mathbb{R}^{6 \times 6}$ with, for $\alpha, \beta = 1, \dots, 6$,

$$(5.1) \quad A_{\alpha\beta}(T) := \int_T D^2\phi_\alpha : D^2\phi_\beta \, dx = |T| (D^2\phi_\alpha : D^2\phi_\beta).$$

LEMMA 5.1. *Let the array $\mathbf{area4e} \in \mathbb{R}^{|\mathcal{T}|}$ contain the area $|T|$ of each triangle $T \in \mathcal{T}$. The following lines of MATLAB compute (5.1).*

```
Integrand = sum(Hessian .* permute(Hessian, [1 2 4 3]), [1 2]);
A4e(:, :, e) = area4e(e) * squeeze(Integrand);
```

Proof. The pairwise Frobenius scalar products of the Hessian matrices $D^2\phi_\alpha$, $\alpha = 1, \dots, 6$ from the array **Hessian** provide the array **Integrand** $\in \mathbb{R}^{6 \times 6}$. The multiplication with the area completes the computation of (5.1). \square

The local contribution $b(T) \in \mathbb{R}^6$ from the triangle $T \in \mathcal{T}$ to the right-hand side consists of approximations to the integral $\int_T f\phi_\alpha \, dx$ for $\alpha = 1, \dots, 6$. Its computation employs the edge-oriented midpoint quadrature rule

$$(5.2) \quad b_\alpha(T) := \frac{|T|}{3} \sum_{\ell=1}^3 f(M_\ell)\phi_\alpha(M_\ell) = \begin{cases} 0 & \text{for } \alpha = 1, 2, 3, \\ |T| f(M_{\alpha-3}) & \text{for } \alpha = 4, 5, 6. \end{cases}$$

LEMMA 5.2. *Let the rows of the array $\mathbf{n4s} \in \mathbb{N}^{|\mathcal{E}| \times 2}$ specify the global numbers of the two endpoints of each edge. Its order determines an enumeration of the edges of the triangulation and the numbers of the three edges of each triangle form the rows of an array $\mathbf{s4e} \in \mathbb{N}^{|\mathcal{T}| \times 3}$. Given a function handle f describing the right-hand side $f : \bar{\Omega} \rightarrow \mathbb{R}$, the evaluations of f required for (5.2) read*

```
f4mid = f((c4n(n4s(:,1), :) + c4n(n4s(:,2), :)) / 2);
valF4e = f4mid(s4e);
```

On the triangle T with index \mathbf{e} , the following lines of MATLAB compute (5.2).

```
b4e(:, e) = [zeros(1, 3), area4e(e) / 3 * valF4e(e, :)];
```

Proof. The right-hand side f is evaluated in the midpoints of each edge first. The array **s4e** allows to select the three point evaluations of f on each triangle into the array **valF4e** $\in \mathbb{R}^{|\mathcal{T}| \times 3}$. On the triangle T , the multiplication with the quadrature weights completes the computation of (5.2). \square

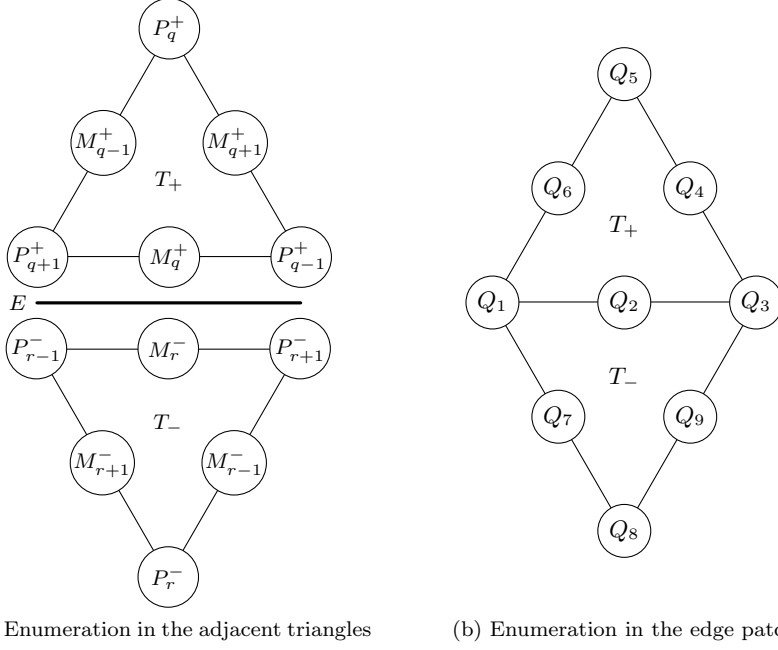


FIG. 2. Local enumeration of nodes associated to the piecewise quadratic basis functions in the adjacent triangles T_+ and T_- and in the whole patch ω_E of the edge E . The local enumeration in each triangle from Figure 1a induces the choice two indices $q, r \in \{1, 2, 3\}$ such that $\text{mid}(E) = M_q^+ = M_r^-$.

6. Jump. This section presents the MATLAB realization of averages and jumps of the derivatives from Section 4 as well as the local contributions to the bilinear form \mathcal{J} . Let $E \in \mathcal{E}$ denote the edge of global number $\mathbf{s} \in \{1, \dots, |\mathcal{E}|\}$, i.e, the global indices of its two vertices belong to the \mathbf{s} -th row of the array $\mathbf{n4s}$.

If $E \in \mathcal{E}(\Omega)$ is an interior edge, two adjacent triangles $T_+, T_- \in \mathcal{T}$ share the edge $\partial T_+ \cap \partial T_- = E$. The local enumeration of the interpolation nodes $P_1^\pm, P_2^\pm, P_3^\pm, M_1^\pm, M_2^\pm, M_3^\pm$ in T_\pm from Figure 1a determine two indices $q, r \in \{1, 2, 3\}$ fixed for each edge E such that $\text{mid}(E) = M_q^+ = M_r^-$. The remaining nodes are numbered accordingly in counter-clockwise order as displayed in Figure 2a in a cyclic notation with index 0 resp. 1 identified with 3 resp. 4. This information is stored in an array $\text{Ind} \in \mathbb{N}^{6 \times 2}$ containing the corresponding permutations of $\{1, \dots, 6\}$ as a column vector or T_+ and T_- . Abbreviate the nodes belonging to the edge patch ω_E for $E \in \mathcal{E}(\Omega)$ by

$$(6.1) \quad \begin{aligned} [Q_1, Q_2, Q_3] &:= [P_{q+1}^+, M_q^+, P_{q-1}^+] = [P_{r-1}^-, M_r^-, P_{r+1}^-], \\ [Q_4, \dots, Q_9] &:= [M_{q+1}^+, P_q^+, M_{q-1}^+, M_{r+1}^-, P_r^-, M_{r-1}^-]. \end{aligned}$$

The nine global basis functions $\phi_1, \dots, \phi_9 \in S^2(\mathcal{T})$ of the edge patch ω_E are associated to the nodes Q_1, \dots, Q_9 as in Figure 2b. This means that ϕ_1, ϕ_2, ϕ_3 belong to the edge E , ϕ_4, ϕ_5, ϕ_6 exclusively to T_+ , and ϕ_7, ϕ_8, ϕ_9 exclusively to T_- . For $\alpha = 1, \dots, 9$, abbreviate the restrictions $\phi_\alpha^\pm := \phi_\alpha|_{T_\pm} \in P_2(T_\pm)$ of ϕ_α to T_\pm .

In the case of a boundary edge $E \in \mathcal{E}(\partial\Omega)$, the nodes Q_7, Q_8, Q_9 corresponding to T_- are omitted and the basis functions $\phi_\alpha := 0$ vanish for $\alpha = 7, 8, 9$.

The evaluations of the normal jumps of the gradients $\nabla\phi_1, \dots, \nabla\phi_9$ in the nodes

Q_1, Q_2, Q_3 on the edge E read, for $\alpha = 1, \dots, 9$ and $\ell = 1, 2, 3$,

$$(6.2) \quad [\nabla\phi_\alpha(Q_\ell) \cdot \nu_E]_E = \begin{cases} (\nabla\phi_\alpha^+(Q_\ell) - \nabla\phi_\alpha^-(Q_\ell)) \cdot \nu_E & \text{if } E \in \mathcal{E}(\Omega), \\ \nabla\phi_\alpha^+(Q_\ell) \cdot \nu_E & \text{if } E \in \mathcal{E}(\partial\Omega), \end{cases}$$

In particular, the vanishing tangential component of the gradient jumps from (3.7) shows

$$(6.3) \quad [\nabla\phi_\beta(Q_2)]_E = [\nabla\phi_\beta(Q_2) \cdot \nu_E]_E \nu_E.$$

LEMMA 6.1. *Let the rows of the array `normal4s` $\in \mathbb{R}^{|\mathcal{E}| \times 2}$ contain the two components of the unit normal vector $\nu_E \in \mathbb{R}^2$ for each edge E . Assume that its sign is chosen such that $\nu_E = \nu_{T_+}$ for the outward unit normal vector ν_{T_+} of the triangle T_+ . Using the five-dimensional array `Grad4s` from Remark 4.4, the following lines of MATLAB compute the jumps (6.2)–(6.3).*

```
GradNormal = squeeze(sum(Grad4s(:,:, :, :), s) .* normal4s(s,:), 2);
JumpNormal = [GradNormal(Ind(1:3,1), Ind(1:3,1), 1) ...
              - GradNormal(Ind(3:-1:1,2), Ind(3:-1:1,2), 2); ...
              GradNormal(Ind(4:6,1), Ind(1:3,1), 1); ...
              - GradNormal(Ind(4:6,2), Ind(3:-1:1,2), 2)];
JumpGrad = JumpNormal(:, 2) * normal4s(s, :);
```

Proof. The array `GradNormal` $\in \mathbb{R}^{6 \times 6 \times 2}$ contains the evaluations of the normal derivatives $\nabla\phi_\alpha^\pm \cdot \nu_E$ for $\alpha = 1, \dots, 6$ at the nodes $P_1^\pm, P_2^\pm, P_3^\pm, M_1^\pm, M_2^\pm, M_3^\pm$ on T_\pm . Their linear combination lead to the jumps along the edge in the array `JumpNormal` $\in \mathbb{R}^{9 \times 3}$ for the basis functions ϕ_α associated to the nodes Q_α for $\alpha = 1, \dots, 9$. The first three basis functions ϕ_1, ϕ_2, ϕ_3 belong to the edge E and the jump consists of the difference of contributions from T_+ and T_- . The array `Ind` selects the corresponding basis functions on the adjacent triangles as well as the corresponding nodes Q_1, Q_2, Q_3 belonging to the edge E . Note that `GradNormal` vanishes on T_- for boundary edges. The basis functions ϕ_4, ϕ_5, ϕ_6 vanish on T_- and the jump of their normal derivatives from T_+ is computed with 0. Vice versa, the basis functions ϕ_7, ϕ_8, ϕ_9 lead to the jump of 0 with the normal derivatives from T_- .

The selection of the evaluation in Q_2 and the multiplication with the unit normal vector ν_E in `normal4s` realize the computation of (6.3) for `JumpGrad` $\in \mathbb{R}^{9 \times 2}$. \square

The averages of the piecewise Hessian matrices from (4.3) read, for $\alpha = 1, \dots, 9$,

$$(6.4) \quad \langle D_{\text{pw}}^2 \phi_\alpha \nu_E \rangle_E = \begin{cases} \frac{1}{2}(D^2\phi_\alpha^+ + D^2\phi_\alpha^-) \nu_E & \text{if } E \in \mathcal{E}(\Omega), \\ D^2\phi_\alpha^+ \nu_E & \text{if } E \in \mathcal{E}(\partial\Omega). \end{cases}$$

LEMMA 6.2. *Let the boolean array `isInteriorSide` $\in \{0, 1\}^{|\mathcal{E}|}$ determine whether an edge belongs to the interior of the domain. The following lines of MATLAB compute the average (6.4).*

```
HessNormal = squeeze(sum(Hess4s(:,:, :, :), s) .* normal4s(s,:), 2);
MeanHessNormal = ...
  [HessNormal(Ind(1:3,1), :, 1) + HessNormal(Ind(3:-1:1,2), :, 2); ...
   HessNormal(Ind(4:6,1), :, 1); HessNormal(Ind(4:6,2), :, 2)];
if isInteriorSide(s); MeanHessNormal = MeanHessNormal / 2; end
```

Proof. The array `HessNormal` $\in \mathbb{R}^{6 \times 2 \times 2}$ contains the product $(\nu_E^\top D^2\phi_\alpha^\pm)^\top = D^2\phi_\alpha^\pm \nu_E$ of each Hessian matrix $D^2\phi_\alpha^\pm$ for $\alpha = 1, \dots, 6$ on T_+ and T_- with the unit

normal vector ν_E . The linear combination for the averages $\langle D_{\text{pw}}^2 \phi_\alpha \nu_E \rangle_E$ along E for $\alpha = 1, \dots, 9$ is computed analogously to `JumpNormal` in the proof of Lemma 6.1 with constant Hessian matrices replacing the gradient evaluations. The two components of the vector-valued averages are stored in the array `MeanHessNormal` $\in \mathbb{R}^{9 \times 2}$. Finally, the prefactor 1/2 is applied for interior edges only according to (6.4). \square

The contribution to the bilinear form \mathcal{J} from the edge $E \in \mathcal{E}$ consists of the local matrix $J(E) \in \mathbb{R}^{9 \times 9}$ with, for $\alpha, \beta = 1, \dots, 9$,

$$(6.5) \quad J_{\alpha\beta}(E) := \int_E \langle D_{\text{pw}}^2 \phi_\alpha \nu_E \rangle_E \cdot [\nabla \phi_\beta]_E \, ds = |E| \langle D_{\text{pw}}^2 \phi_\alpha \nu_E \rangle_E \cdot [\nabla \phi_\beta(Q_2)]_E.$$

If $E \in \mathcal{E}(\partial\Omega)$, $\phi_7, \phi_8, \phi_9 \equiv 0$ implies that $J_{\alpha\beta}(E) = 0$ vanishes for all $\alpha, \beta = 1, \dots, 9$ with $7 \leq \alpha$ or $7 \leq \beta$.

LEMMA 6.3. *Let the array `length4s` $\in \mathbb{R}^{|\mathcal{E}|}$ contain the length of each edge. The following line of MATLAB computes (6.5).*

```
J4s(:, :, s) = length4s(s) * (MeanHessNormal * JumpGrad');
```

Proof. The pairwise scalar products for $\alpha, \beta = 1, \dots, 9$ of the evaluations from the Lemmas 6.2–6.1 followed by the multiplication with the length of the edge E realize to the computation of the integral in (6.5). \square

7. Penalization. Recall the enumeration of nodes and basis functions in the edge patch ω_E from Section 6.

LEMMA 7.1. *Given a parameter $\mathbf{a} := a > 1$, the following lines of MATLAB compute the automatic penalization parameter $\sigma_{\text{IP},E}$ from (1.8).*

```
sigma4s = 3 * a * (length4s.^2) ./ area4e(e4s(:,1));
sigma4s(isInteriorSide) = sigma4s(isInteriorSide) / 4 ...
+ 3/4 * a * length4s(isInteriorSide).^2 ...
./ area4e(e4s(isInteriorSide,2));
```

Proof. The parameter $\sigma_{\text{IP},E}$ consists of the sum of one contribution from each adjacent triangle T_+ and T_- . The value for all edges $E \in \mathcal{E}$ is initialized by $3a h_E^2 / |T_+|$. In case of an interior edge, the contribution from T_+ is multiplied with the prefactor 1/4 and the term $3a h_E^2 / (4|T_-|)$ for T_- is added. \square

The contribution to the penalty term c_{IP} from the edge $E \in \mathcal{E}$ leads to the local matrix $C(E) \in \mathbb{R}^{9 \times 9}$ with, for $\alpha, \beta = 1, \dots, 9$,

$$C_{\alpha\beta}(E) := \frac{\sigma_{\text{IP},E}}{h_E} \int_E [\nabla \phi_\alpha \cdot \nu_E]_E [\nabla \phi_\beta \cdot \nu_E]_E \, ds.$$

The three-point one-dimensional Simpson quadrature rule with quadrature nodes Q_1, Q_2, Q_3 from (6.1) and weights $w_1 = w_3 = 1/6$ and $w_2 = 2/3$ integrates the product of the jump terms exactly and reads

$$(7.1) \quad C_{\alpha\beta}(E) = \sigma_{\text{IP},E} \sum_{j=1}^3 w_j [\nabla \phi_\alpha(Q_j) \cdot \nu_E]_E [\nabla \phi_\beta(Q_j) \cdot \nu_E]_E.$$

If $E \in \mathcal{E}(\partial\Omega)$, $\phi_7, \phi_8, \phi_9 \equiv 0$ implies that $C_{\alpha\beta}(E) = 0$ vanishes for all $\alpha, \beta = 1, \dots, 9$ with $7 \leq \alpha$ or $7 \leq \beta$.

LEMMA 7.2. *The following lines of MATLAB compute (7.1).*

```
Integrand = JumpNormal .* permute(JumpNormal, [3 2 1]);
C4s(:, :, s) = sigma4s(s)/6 * squeeze(sum([1 4 1] .* Integrand, 2));
```

Proof. The pairwise products of the evaluations of the normal jumps $[\nabla\phi_\alpha \cdot \nu_E]_E$, $\alpha = 1, \dots, 9$, in `JumpNormal` from Lemma 6.1 form the array `Integrand` $\in \mathbb{R}^{9 \times 3 \times 9}$. The multiplication with the penalty parameter $\sigma_{\text{IP}, E}$ and the quadrature weights followed by the sum over the three terms of the quadrature rule complete the computation of (7.1). \square

8. Assembling. This section describes the assembling of the global system matrix using the local contributions from the Sections 5–7. To this end, let $\mathcal{V} = \{z_1, \dots, z_K\}$ denote a global enumeration of the $K := |\mathcal{V}| \in \mathbb{N}$ vertices and $\mathcal{E} = \{E_1, \dots, E_L\}$ of the $L := |\mathcal{E}| \in \mathbb{N}$ edges of the triangulation \mathcal{T} . The edge midpoints $\text{mid}(\mathcal{E}) = \{m_\ell := \text{mid}(E_\ell) : \ell = 1, \dots, L\}$ are numbered accordingly. This induces a global enumeration of the $N := N := K + L$ basis functions $\varphi_1, \dots, \varphi_N \in S^2(\mathcal{T})$ via, for all $j, k = 1, \dots, K$ and $\ell, n = 1, \dots, L$,

$$\varphi_j(z_k) = \delta_{jk}, \quad \varphi_{K+\ell}(m_n) = \delta_{\ell n}, \quad \text{and} \quad \varphi_j(m_n) = 0 = \varphi_{K+\ell}(z_k).$$

The bilinear form a_{pw} leads to the global stiffness matrix $A \in \mathbb{R}^{N \times N}$ with

$$A_{jk} := a_{\text{pw}}(\varphi_j, \varphi_k) = \sum_{T \in \mathcal{T}} \int_T \text{D}^2 \varphi_j : \text{D}^2 \varphi_k \, dx \quad \text{for all } j, k = 1, \dots, N.$$

The integration of the right-hand side $\int_\Omega f \varphi_j \, dx$ from (1.4) employs the edge-oriented midpoint quadrature rule. The resulting right-hand side vector $b \in \mathbb{R}^N$ reads, for all $j = 1, \dots, K$ and $\ell = 1, \dots, L$,

$$b_j := 0 \quad \text{and} \quad b_{K+\ell} := \sum_{T \in \mathcal{T}, E_\ell \subset T} \frac{|T|}{3} f(\text{mid}(E_\ell)).$$

The assembling of A and b with the local contributions $A(T)$ and $b(T)$ from Section 5 requires the translation of local indices of shape functions on the triangle $T \in \mathcal{T}$ into global indices of basis functions. The index set

$$I(T) := \{(\alpha, j) \in \{1, 2, 3\} \times \{1, \dots, K\} : P_\alpha = z_j\} \\ \cup \{(3 + \alpha, K + \ell) : (\alpha, \ell) \in \{1, 2, 3\} \times \{1, \dots, L\} \text{ with } M_\alpha = m_\ell\}.$$

is stored in the variable `dof4e = [n4e, nNodes + s4e]` in that the index j has position α in the column associated to T and analogously for $K + \ell$ and $3 + \alpha$. The set $I(T)$ leads to the assembling of $A \in \mathbb{R}^{N \times N}$ and $b \in \mathbb{R}^N$ via

$$(8.1) \quad A = \sum_{T \in \mathcal{T}} \sum_{(\alpha, j) \in I(T)} \sum_{(\beta, k) \in I(T)} A_{\alpha\beta}(T) e_j \otimes e_k,$$

$$(8.2) \quad b = \sum_{T \in \mathcal{T}} \sum_{(\alpha, j) \in I(T)} b_\alpha(T) e_j.$$

LEMMA 8.1. *The following lines of MATLAB compute A and b from (8.1)–(8.2).*

```
RowIndices4e = permute( repmat(dof4e, [1 1 size(dof4e, 2)]), [1 3 2]);
ColIndices4e = permute( RowIndices4e, [2 1 3]);
A = sparse(RowIndices4e(:), ColIndices4e(:), A4e(:), N, N);
b = accumarray(dof4e(:), b4e(:), [N 1]);
```

Proof. The indices of $I(T)$ in `dof4e` are rearranged to match the requirements of MATLAB's `sparse` command. This results in the two arrays `RowIndices4e`, `ColIndices4e` $\in \mathbb{N}^{6 \times 6 \times |T|}$ of the same size as `A4e`. For each entry in `A4e`, the corresponding entries in `RowIndices4e` and `ColIndices4e` provide the row and column indices of the global position in `A`. The `accumarray` function realizes the same procedure for dense one-dimensional arrays. \square

The bilinear forms \mathcal{J} and c_{IP} lead to the global matrices $J \in \mathbb{R}^{N \times N}$ and $C \in \mathbb{R}^{N \times N}$ with, for all $j, k = 1, \dots, N$,

$$J_{jk} := \mathcal{J}(\varphi_j, \varphi_k) = \sum_{E \in \mathcal{E}} \int_E \langle D_{\text{pw}}^2 \varphi_j \nu_E \rangle_E \cdot [\nabla \varphi_k]_E \, ds,$$

$$C_{jk} := c_{\text{IP}}(\varphi_j, \varphi_k) = \sum_{E \in \mathcal{E}} \frac{\sigma_{\text{IP}, E}}{h_E} \int_E [\nabla \varphi_j \cdot \nu_E]_E [\nabla \varphi_k \cdot \nu_E]_E \, ds.$$

Recall the enumeration of the nodes Q_1, \dots, Q_9 from (6.1) as displayed in Figure 2. The translation of local indices of shape functions on the edge patch ω_E into global indices of basis functions employs the index sets $I(E) := I^+(E) \cup I^-(E)$ defined by

$$I^+(E) := \{(\alpha, j) \in \{1, 3, 5\} \times \{1, \dots, K\} : Q_\alpha = z_j\} \\ \cup \{(\alpha, M + \ell) : \alpha \in \{2, 4, 6\}, \ell \in \{1, \dots, L\}, Q_\alpha = m_\ell\}$$

and $I^-(E)$ according to the location of E . For an interior edge $E \in \mathcal{E}(\Omega)$, the indices from T_- read

$$I^-(E) := \{(8, j) : j \in \{1, \dots, K\}, Q_8 = z_j\} \\ \cup \{(\alpha, K + \ell) : \alpha \in \{7, 9\}, \ell \in \{1, \dots, K\}, Q_\alpha = m_\ell\}.$$

For a boundary edge $E \in \mathcal{E}(\partial\Omega)$, recall that the local contributions $J_{\alpha\beta}(E) = C_{\alpha\beta}(E) = 0$ from the Sections 6 and 7 vanish for all $\alpha, \beta = 1, \dots, 9$ with $7 \leq \alpha$ or $7 \leq \beta$. The vanishing entries do not influence the assembling of the global matrix and the corresponding index pairs can be chosen arbitrarily, e.g., $I^-(E) := \{(7, 1), (8, 1), (9, 1)\}$. The set $I(E)$ is stored in a variable `dof4s` $\in \mathbb{N}^{|\mathcal{E}| \times 9}$ similarly to `dof4e` for $I(T)$. For the detailed realization, the reader is referred to the lines 23–41 of the code in the Appendix A. The assembling of $J \in \mathbb{R}^{N \times N}$ with the local contributions $J(E)$ from Section 6 reads

$$(8.3) \quad J = \sum_{E \in \mathcal{E}} \sum_{(\alpha, j) \in I(E)} \sum_{(\beta, k) \in I(E)} J_{\alpha\beta}(E) e_j \otimes e_k,$$

and analogously for $C \in \mathbb{R}^{N \times N}$ with $C_{\alpha\beta}(E)$ from Section 7 replacing $J_{\alpha\beta}(E)$. The MATLAB realization of (8.3) is verbatim to Lemma 8.1 with `dof4s` replacing `dof4e`.

The sum of the three contributions results in the system matrix

$$B := A - J - J^\top + C \in \mathbb{R}^{N \times N}.$$

Since the discrete solution $u_{\text{IP}} \in S_0^2(\mathcal{T})$ to (1.4) vanishes along the boundary, the indices of the degrees of freedom in the set

$$I(\Omega) := \{j \in \{1, \dots, M\} : z_j \in \mathcal{V}(\Omega)\} \cup \{M + \ell : \ell \in \{1, \dots, L\}, E_\ell \in \mathcal{E}(\Omega)\}$$

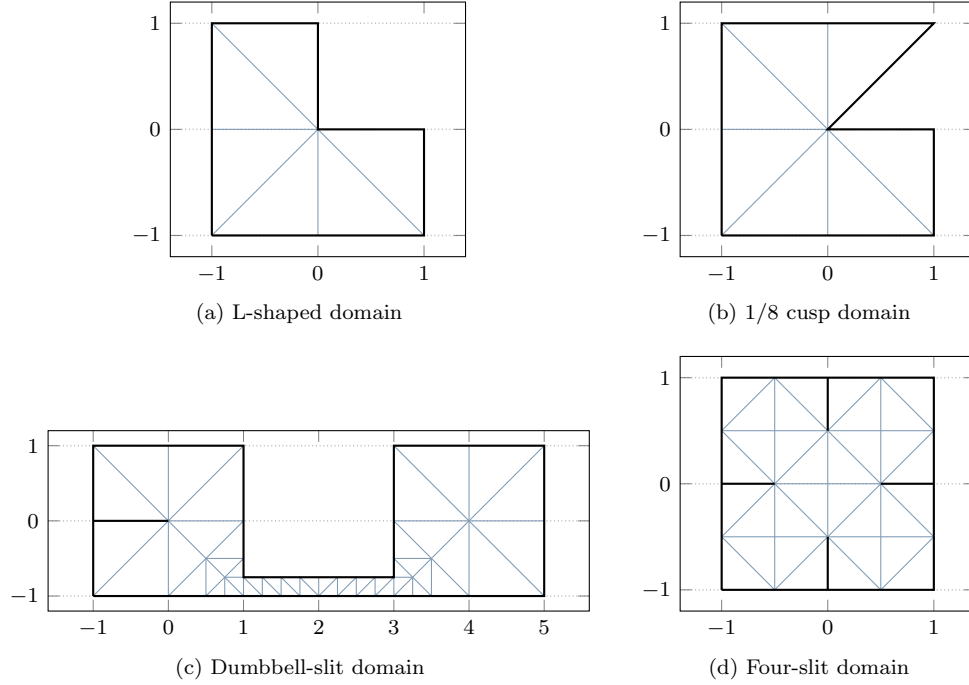


FIG. 3. Visualization of the initial triangulations \mathcal{T}_0 for the four benchmark problems.

restrict to all interpolation nodes in the interior of the domain. The discrete formulation (1.4) seeks the coefficient vector $x \in \mathbb{R}^{M+L}$ of

$$u_{\text{IP}} = \sum_{j=1}^{M+L} x_j \varphi_j \in S_0^2(\mathcal{T})$$

with $x_j = 0$ for all boundary indices $j \in \{1, \dots, M+L\} \setminus I(\Omega)$ satisfying the linear system of equations

$$(B_{jk})_{j,k \in I(\Omega)} (x_k)_{k \in I(\Omega)} = (b_j)_{j \in I(\Omega)}.$$

The solution of this system concludes the realization of the C^0 interior penalty method from (1.4).

9. Numerical experiments. This section investigates the implementation from Appendix A for four computational benchmark examples with domains in Figure 3.

The experiments focus on a comparison of uniform and adaptive mesh-refinement driven by the a posteriori error estimator η from Appendix B below. This employs the Dörfler marking strategy [17] and newest-vertex bisection according to [23] in the adaptive Algorithm 9.1. The marking strategy with minimal cardinality of the set \mathcal{M}_ℓ of marked triangles can be realized in linear computational complexity [22].

Another main aspect of the numerical investigation concerns the nonparametric choice of the stabilization introduced in Section 3. To this end, the principal eigenvalue λ_1 to the following eigenvalue problem is computed: Seek $(\Phi_{\text{IP}}, \mu) \in V_h \times \mathbb{R}$ such that $\Phi_{\text{IP}} \neq 0$ and

$$(9.1) \quad A_h(\Phi_{\text{IP}}, v_{\text{IP}}) = \mu(a_{\text{pw}}(\Phi_{\text{IP}}, v_{\text{IP}}) + c_{\text{IP}}(\Phi_{\text{IP}}, v_{\text{IP}})) \quad \text{for all } v_{\text{IP}} \in V_h.$$

Algorithm 9.1 Adaptive C⁰ interior penalty method**Input:** regular triangulation \mathcal{T}_0 and bulk parameter $0 < \theta \leq 1$.**for** $\ell = 0, 1, 2, \dots$ **do** **Solve** (1.4) with respect to triangulation \mathcal{T}_ℓ for solution $u_\ell \in S_0^2(\mathcal{T}_\ell)$. **Compute** refinement indicator $\eta^2(\mathcal{T}_\ell, T)$ from (B.1) for all $T \in \mathcal{T}_\ell$. **Mark** a minimal subset $\mathcal{M}_\ell \subseteq \mathcal{T}_\ell$ by the Dörfler criterion

$$\theta \eta^2(\mathcal{T}_\ell) \leq \sum_{T \in \mathcal{M}_\ell} \eta^2(\mathcal{T}_\ell, T).$$

Refine \mathcal{T}_ℓ to $\mathcal{T}_{\ell+1}$ by newest-vertex bisection such that $\mathcal{M}_\ell \subseteq \mathcal{T}_\ell \setminus \mathcal{T}_{\ell+1}$.**end for****Output:** sequence of triangulations \mathcal{T}_ℓ with u_ℓ and $\eta(\mathcal{T}_\ell)$ for $\ell \in \mathbb{N}_0$.

The practical implementation employs MATLAB's `eigs` function in one line.

```
[~, lambda] = eigs(B(dof,dof), A(dof,dof) + C(dof,dof), 1, 0);
```

The Rayleigh-Ritz principle shows that the principal eigenvalue λ_1 is an upper bound for the stability constant $\kappa = 1/2$ in the case of $a = 4$ in Theorem 3.1.

9.1. Singular solution on the L-shaped domain. This benchmark considers the L-shaped domain $\Omega = (-1, 1)^2 \setminus [0, 1)^2$ with interior angle $\omega = 3\pi/2$ at the reentrant corner. This determines the noncharacteristic solution $\alpha := 0.5444837$ with $\sin^2(\alpha\omega) = \alpha^2 \sin^2(\omega)$ in

$$(9.2) \quad g_{\alpha,\omega}(\varphi) = \left(\frac{\sin((\alpha-1)\omega)}{\alpha-1} - \frac{\sin((\alpha+1)\omega)}{\alpha+1} \right) (\cos((\alpha-1)\varphi) - \cos((\alpha+1)\varphi)) \\ - \left(\frac{\sin((\alpha-1)\varphi)}{\alpha-1} - \frac{\sin((\alpha+1)\varphi)}{\alpha-1} \right) (\cos((\alpha-1)\omega) - \cos((\alpha+1)\omega)).$$

The exact singular solution in polar coordinates from [20, p. 107] reads

$$(9.3) \quad u(r, \varphi) = (1 - r^2 \cos^2 \varphi)^2 (1 - r^2 \sin^2 \varphi)^2 r^{1+\alpha} g_{\alpha,\omega} \left(\varphi - \frac{\pi}{2} \right).$$

The right-hand side $f := \Delta^2 u$ is computed accordingly. The reduced regularity of the exact solution u leads to the empirical convergence rate $\alpha/2$ for uniform mesh-refinement displayed by dashed lines in Figure 5. The adaptive refinement strategy results in local mesh-refining at the reentrant corner and recovers the optimal convergence rate $1/2$ with respect to the number of degrees of freedom (ndof) displayed by the solid lines in Figure 5.

9.2. Singular solution on the 1/8 cusp domain. This benchmark problem investigates the 1/8 cusp domain $\Omega := (-1, 1)^2 \setminus \text{conv}\{(0, 0), (1, -1), (1, 0)\}$ with interior angle $\omega = 7\pi/4$ as depicted in Figure 3b. The right-hand side $f := \Delta^2 u$ is given by the exact singular solution in polar coordinates

$$(9.4) \quad u(r, \varphi) = (1 - r^2 \cos^2 \varphi)^2 (1 - r^2 \sin^2 \varphi)^2 r^{1+\alpha} g_{\alpha,\omega} \left(\varphi - \frac{\pi}{4} \right)$$

analogously to (9.3) with $g_{\alpha,\omega}$ from (9.2) for the parameter $\alpha = 0.50500969$. The singularity causes an empirical convergence rate $\alpha/2$ for uniform mesh-refinement in

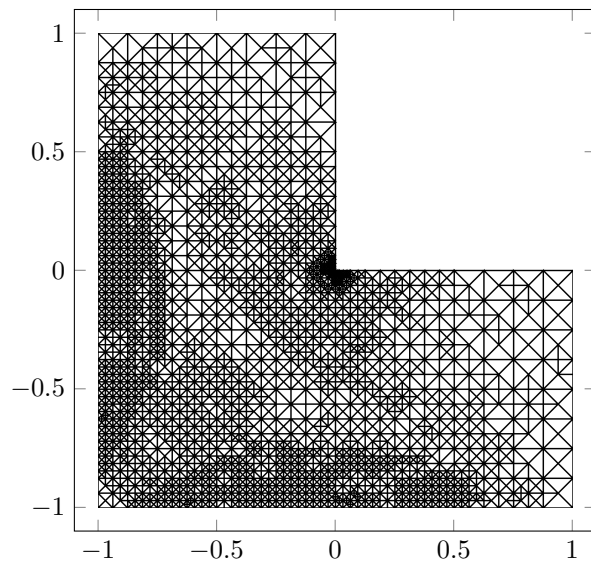


FIG. 4. *Adaptively refined mesh ($\theta = 0.5$) with 10406 degrees of freedom for the L-shaped domain from Section 9.1.*

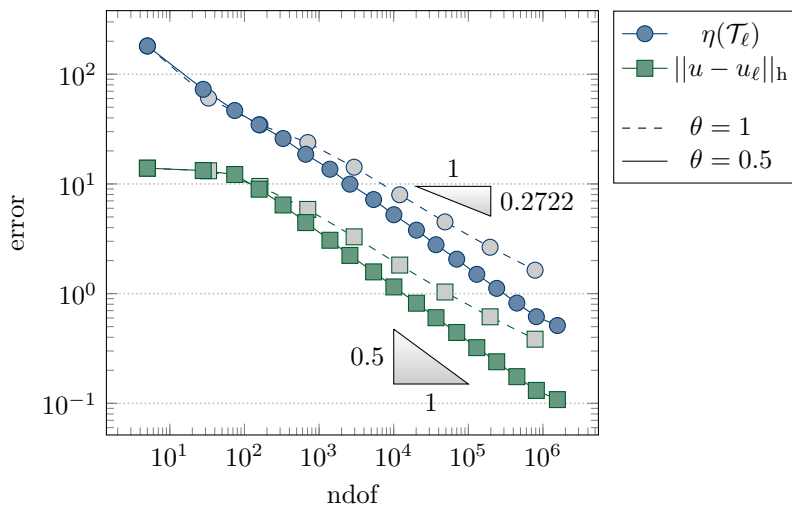


FIG. 5. *Convergence history plot for the benchmark problem on the L-shaped domain from Section 9.1.*

Figure 6, while the adaptive algorithm recovers the optimal rate $1/2$. Undisplayed triangulation plots confirm the increased adaptive refinement towards the reentrant corner.

9.3. Uniform load on the dumbbell-slit domain. The benchmark problem applies the uniform force $f \equiv 1$ on the dumbbell-slit domain

$$\Omega = \left((-1, 1) \times (-1, 5) \setminus [1, 3] \times [-0.75, 1) \right) \setminus (-1, 0] \times \{0\}$$

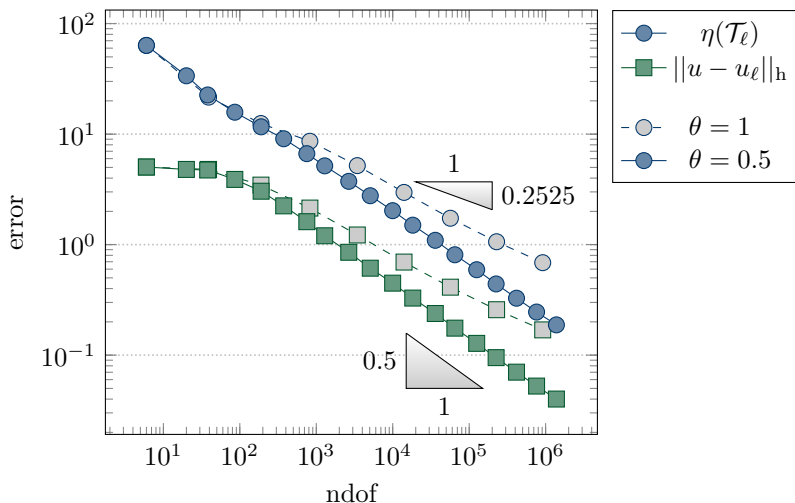


FIG. 6. Convergence history plot for the benchmark problem on the 1/8 cusp domain from Section 9.2.

depicted in Figure 3c. Although Ω is no Lipschitz domain, Figures 7c and 8c confirm the optimal convergence rate with adaptive mesh-refinement and the stability result from Theorem 3.1. Undisplayed plots of the adaptive triangulations show an increased refinement towards the slit as well as the two reentrant corners at $(1, -0.75)$ and $(3, -0.75)$.

9.4. Uniform load on the four-slit domain. Let

$$\Omega = \left((-1, 1)^2 \setminus ([-1, -0.5] \cup [0.5, 1]) \times \{0\} \right) \setminus \{0\} \times ([-1, -0.5] \cup [0.5, 1])$$

denote the square domain with one slit at each edge as depicted in Figure 3d. This benchmark also considers the uniform load $f \equiv 1$. Undisplayed triangulation plots indicate that the adaptive algorithm detects the singularities of the unknown exact solution at tips of the four slits.

9.5. Conclusions. While [6] provides a proof of the quasi-optimality of adaptive discontinuous Galerkin schemes for the diffusion problem, a rigorous proof of optimal convergence rates remains open for the biharmonic problem. Nevertheless, the numerical experiments in Figure 7 exhibit rate-optimal convergence of the adaptive C⁰ interior penalty method. In particular, even moderate bulk parameters $\theta \leq 0.75$ in the Dörfler marking in Algorithm 9.1 improve the suboptimal convergence rates for uniform refinement and lead to the optimal rate of 1/2 in all four benchmark problems.

Figure 8 displays the stability constant λ_1 from (9.1) for adaptive and uniform mesh-refinement in all four benchmark problems. The computed values for λ_1 are slightly larger than the guaranteed lower bound 1/2 from Theorem 3.1 for $a = 4$. The graphs tend towards values between 0.6 and 0.7 indicating a small over-stabilization of the automated choice of $\sigma_{\text{IP},E}$. An interesting empirical observation is that adaptive mesh-refinement leads to slightly more stable discretization with larger stability constants. The plots in Figure 8 exhibit no significant difference between the four domains. This supports the advantage of the automated choice of the penalization with $\sigma_{\text{IP},E}$ for guaranteed stability. The proposed automatic parameter selection appears

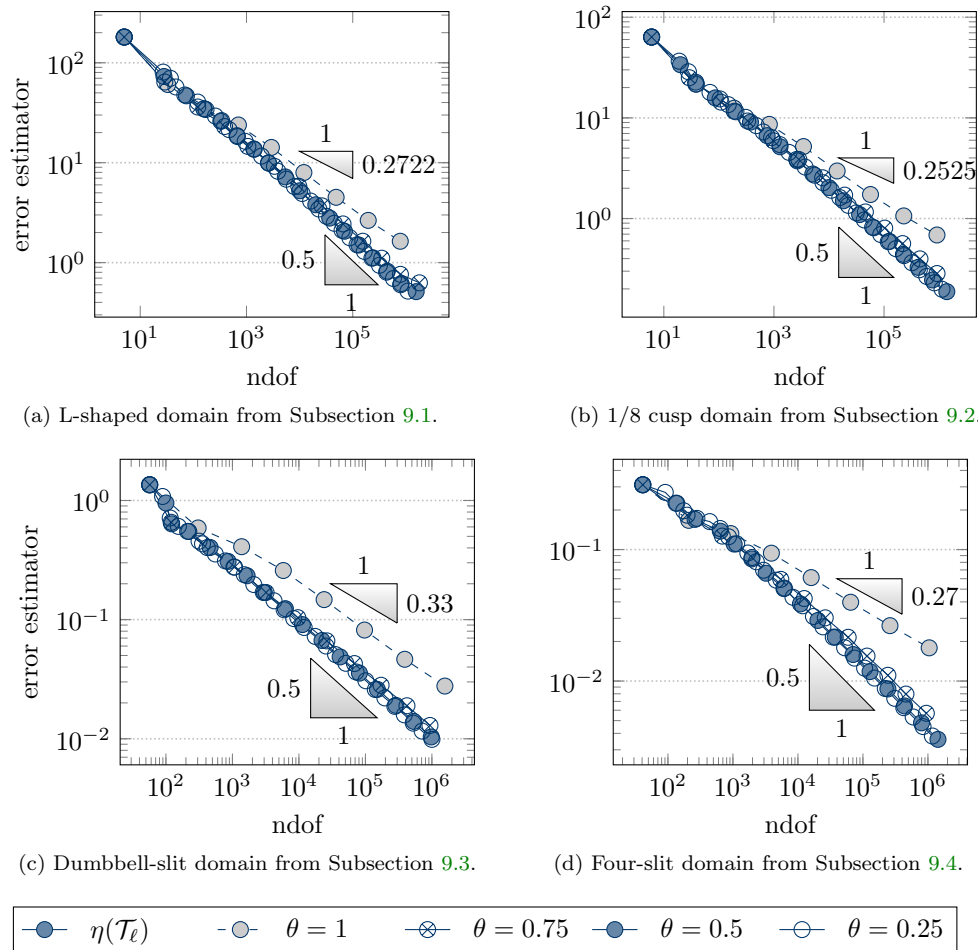


FIG. 7. Convergence history plot of the error estimator η from (B.1) for several choices of the bulk parameters θ .

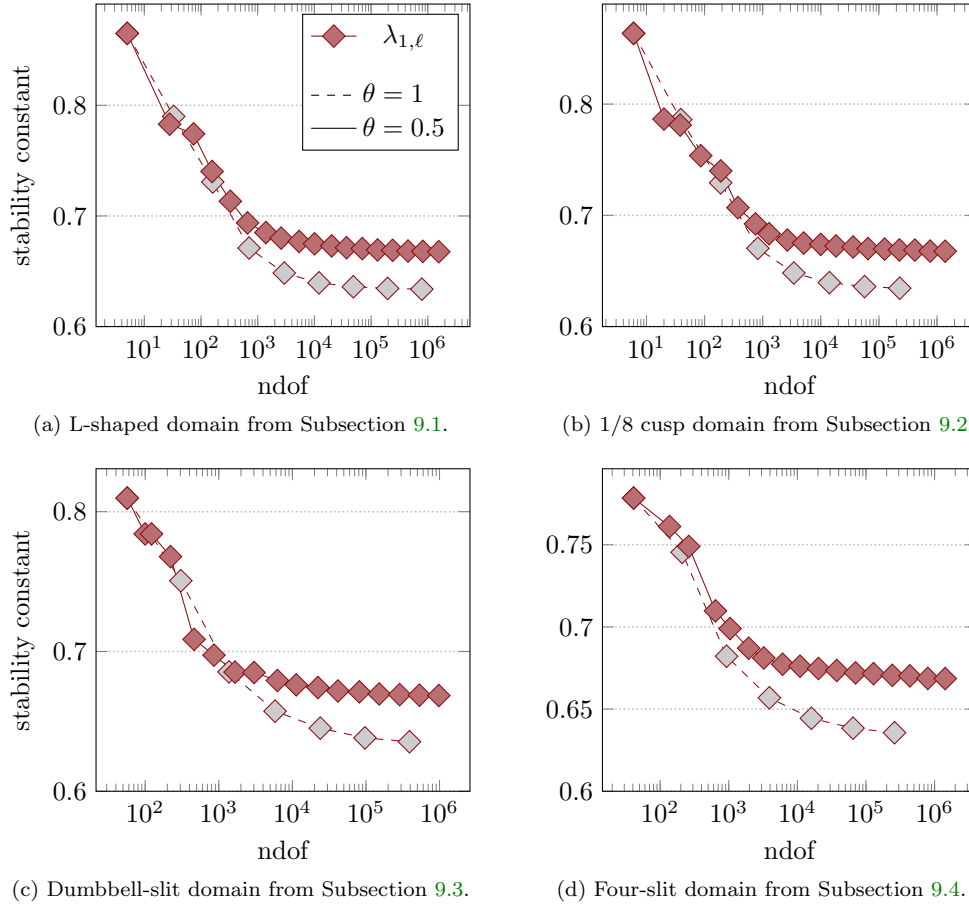
to be compatible with adaptive mesh-refining. An over-stabilization as in [6] is not necessary in the computational benchmarks.

Data availability. Data sharing not applicable as to this article as no datasets were generated or analyzed during the current study.

Declarations. The authors declare that they have no conflict of interests.

REFERENCES

- [1] S. AGMON, *Lectures on elliptic boundary value problems*, AMS Chelsea Publishing, Providence, RI, 2010. Prepared for publication by B. Frank Jones, Jr. with the assistance of George W. Batten, Jr., Revised edition of the 1965 original.
- [2] J. H. ARGYRIS, I. FRIED, AND D. W. SCHARPF, *The tuba family of plate elements for the matrix displacement method*, *Aeronautical Journal*, 72 (1968), pp. 701–709.

FIG. 8. Plot of stability constant $\lambda_{1,\ell}$.

- [3] G. A. BAKER, *Finite element methods for elliptic equations using nonconforming elements*, Math. Comp., 31 (1977), pp. 45–59, <https://doi.org/10.2307/2005779>, <https://doi.org/10.2307/2005779>.
- [4] J. M. BALL AND C. CARSTENSEN, *Interaction of martensitic microstructures in adjacent grains*, in Proceedings of the International Conference on Martensitic Transformations: Chicago, A. P. Stebner and G. B. Olson, eds., Cham, 2018, Springer International Publishing, pp. 29–33.
- [5] H. BLUM AND R. RANNACHER, *On the boundary value problem of the biharmonic operator on domains with angular corners*, Math. Methods Appl. Sci., 2 (1980), pp. 556–581.
- [6] A. BONITO AND R. H. NOCHETTO, *Quasi-optimal convergence rate of an adaptive discontinuous Galerkin method*, SIAM J. Numer. Anal., 48 (2010), pp. 734–771.
- [7] D. BRAESS, *Finite elements*, Cambridge University Press, Cambridge, third ed., 2007. Theory, fast solvers, and applications in elasticity theory, Translated from the German by Larry L. Schumaker.
- [8] S. C. BRENNER, *C^0 interior penalty methods*, in Frontiers in numerical analysis—Durham 2010, vol. 85 of Lect. Notes Comput. Sci. Eng., Springer, Heidelberg, 2012, pp. 79–147.
- [9] S. C. BRENNER AND L. R. SCOTT, *The mathematical theory of finite element methods*, vol. 15 of Texts in Applied Mathematics, Springer, New York, third ed., 2008.
- [10] S. C. BRENNER AND L.-Y. SUNG, *C^0 interior penalty methods for fourth order elliptic boundary value problems on polygonal domains*, J. Sci. Comput., 22/23 (2005), pp. 83–118.
- [11] S. C. BRENNER, L.-Y. SUNG, H. ZHANG, AND Y. ZHANG, *A Morley finite element method for the displacement obstacle problem of clamped Kirchhoff plates*, J. Comput. Appl. Math.,

- 254 (2013), pp. 31–42.
- [12] C. CARSTENSEN, G. MALLIK, AND N. NATARAJ, *A priori and a posteriori error control of discontinuous Galerkin finite element methods for the von Kármán equations*, IMA J. Numer. Anal., 39 (2019), pp. 167–200.
- [13] C. CARSTENSEN AND N. NATARAJ, *Adaptive Morley FEM for the von Kármán equations with optimal convergence rates*, SIAM J. Numer. Anal., 59 (2021), pp. 696–719.
- [14] C. CARSTENSEN AND N. NATARAJ, *A priori and a posteriori error analysis of the Crouzeix-Raviart and Morley FEM with original and modified right-hand sides*, Comput. Methods Appl. Math., 21 (2021), pp. 289–315.
- [15] C. CARSTENSEN AND N. NATARAJ, *Lowest-order equivalent nonstandard finite element methods for biharmonic plates*, ESAIM Math. Model. Numer. Anal., 56 (2022), pp. 41–78.
- [16] D. A. DI PIETRO AND A. ERN, *Mathematical aspects of discontinuous Galerkin methods*, vol. 69, Springer, 2011.
- [17] W. DÖRFLER, *A convergent adaptive algorithm for Poisson’s equation*, SIAM J. Numer. Anal., 33 (1996), pp. 1106–1124.
- [18] D. GALLISTL, *Morley finite element method for the eigenvalues of the biharmonic operator*, IMA J. Numer. Anal., 35 (2015), pp. 1779–1811.
- [19] D. GILBARG AND N. S. TRUDINGER, *Elliptic partial differential equations of second order*, Classics in Mathematics, Springer-Verlag, Berlin, 2001. Reprint of the 1998 edition.
- [20] P. GRISVARD, *Singularities in boundary value problems*, vol. 22 of Recherches en Mathématiques Appliquées [Research in Applied Mathematics], Masson, Paris; Springer-Verlag, Berlin, 1992.
- [21] J. NEČAS, *Direct methods in the theory of elliptic equations*, Springer Monographs in Mathematics, Springer, Heidelberg, 2012. Translated from the 1967 French original by Gerard Tronel and Alois Kufner, Editorial coordination and preface by Šárka Nečasová and a contribution by Christian G. Simader.
- [22] C.-M. PFEILER AND D. PRAETORIUS, *Dörfler marking with minimal cardinality is a linear complexity problem*, Math. Comp., 89 (2020), pp. 2735–2752.
- [23] R. STEVENSON, *The completion of locally refined simplicial partitions created by bisection*, Math. Comp., 77 (2008), pp. 227–241.
- [24] E. SÜLI AND I. MOZOLEVSKI, *hp-version interior penalty DGFEMs for the biharmonic equation*, Comput. math. with appl., 196 (2007), pp. 1851–1863.

Appendix A. 116 lines of MATLAB. This section describes the realization of the computations from the Sections 4, 6, 7 and 8 as a single MATLAB function. The code has been implemented and tested with MATLAB version 9.9.0.1718557 (R2020b) Update 6.

```

1 function [u, ndof] = COIP(c4n, n4e, f, a)
   %%COIP solves the biharmonic problem  $\Delta^2 u = f$ 
   %%for a given right-hand side f and clamped boundary condition on the
   %%domain given by the data structures c4n, n4e. The parameter a > 1
   %%is optional and allows a fine tuning of the automatic penalization
   %%parameter (default value a = 4).
   % [u, ndof] = COIP(c4n, n4e, f, a)

   %% PROCEED OPTIONAL INPUT PARAMETER
2 if nargin < 4; a = 4; end

   %% GEOMETRIC INFORMATION
   % Global constants
3 nNodes = size(c4n, 1);
4 nElem = size(n4e, 1);
   % Connectivity information on sides
5 [sortedSides, localPosition] = ...
6     sort([n4e(:, [2 3]); n4e(:, [3 1]); n4e(:, [1 2])], 2);
7 [~, index, position] = unique(sortedSides, 'rows', 'first');
8 n4s = sortedSides(sub2ind(size(sortedSides), repmat(index, 1, 2), ...
9     localPosition(index, :)));
10 nSides = size(n4s, 1);
11 s4e = reshape(position, nElem, 3);
12 ElemNo = repmat((1:nElem)', 3, 1);
13 e4s = [ElemNo(index), accumarray(position, ElemNo) - ElemNo(index)];
14 isInteriorSide = (e4s(:,2) ~= 0);

```

```

% Geometric information on edges
15 tangent4s = c4n(n4s(:,2),:) - c4n(n4s(:,1),:);
16 length4s = sqrt(sum(tangent4s.^2, 2));
17 tangent4s = tangent4s ./ length4s;
18 normal4s = [tangent4s(:,2), - tangent4s(:,1)];
% Geometric information on triangles
19 c4e = permute(reshape(c4n(n4e,:), nElem, 3, 2), [3 2 1]);
20 area4e = squeeze(abs(sum((c4e(2,[2 3 1],:) - c4e(2,[3 1 2],:)) ...
21     .* c4e(1,:,:), 2))) / 2;

%% INDEXING INFORMATION
% Global indexing information for triangles
22 dof4e = [n4e, nNodes + s4e]';
% Local index {1,2,3} of the opposite node in T+ and T-
23 [oppositeIndPlus,~] = ...
24     find(all(n4e(e4s(:,1),:) ~= permute(n4s, [1 3 2]), 3)');
25 [oppositeIndMinus,~] = ...
26     find(all(n4e(e4s(isInteriorSide,2),:) ...
27     ~= permute(n4s(isInteriorSide,:), [1 3 2]), 3)');
% Local enumeration of interpolation nodes in T+ and T-
28 LOCAL = [2 4 3 5 1 6; 3 5 1 6 2 4; 1 6 2 4 3 5]';
29 localInd4s = ones(6, 2, nSides);
30 localInd4s(:,1,:) = LOCAL(:,oppositeIndPlus);
31 localInd4s(:,2,isInteriorSide) = LOCAL(:,oppositeIndMinus);
% Global indexing information for edge patches
32 dof4s = [n4s(:,1), nNodes + (1:nSides)', n4s(:,2), ones(nSides, 6)]';
33 dof4s(5,:) = n4e(sub2ind(size(n4e), e4s(:,1), oppositeIndPlus));
34 dof4s([4 6],:) = nNodes + ...
35     s4e(sub2ind(size(s4e), repmat(e4s(:,1), [1 2]), ...
36     LOCAL([1 3], oppositeIndPlus)'))';
37 dof4s(8,isInteriorSide) = ...
38     n4e(sub2ind(size(n4e), e4s(isInteriorSide,2), oppositeIndMinus));
39 dof4s([7 9],isInteriorSide) = nNodes + ...
40     s4e(sub2ind(size(s4e), repmat(e4s(isInteriorSide,2), [1 2]), ...
41     LOCAL([1 3],oppositeIndMinus)'))';

%% COMPUTATION OF TRIANGLE-ORIENTED LOCAL CONTRIBUTIONS
% Evaluation of right-hand side f in nodes for edge-oriented midpoint
% quadrature rule
42 f4mid = f((c4n(n4s(:,1),:) + c4n(n4s(:,2),:)) / 2);
43 valF4e = f4mid(s4e);
% Evaluation of gradients of quadratic shape functions
% 1st dimension : 6 basis functions
% 2nd dimension : 2 components of gradients
% 3rd dimension : 6 quadrature nodes (3 vertices & 3 edge midpoints)
% 4th dimension : each triangle
44 Grad4e = zeros(6, 2, 6, nElem);
% Evaluation of Hessian of quadratic shape functions
% 1st dimension : 6 basis functions
% 2nd & 3rd dimension : 2-by-2 components of Hessian
% 4th dimension : each triangle
45 Hess4e = zeros(6, 2, 2, nElem);
% Local contributions to stiffness matrix
46 A4e = zeros(6, 6, nElem);
% Local contributions to right-hand side
47 b4e = zeros(6, nElem);

48 parfor e = 1:nElem
% Compute gradients of barycentric coordinates
49     GradP1 = [ones(1,3); c4e(:, :, e)] \ [zeros(1,2); eye(2)];
% Compute Hessian of quadratic shape functions

```

```

50     H = permute(GradP1, [2 3 1 4]) .* permute(GradP1, [3 2 4 1]);
51     Hessian = 4 * cat(3, H(:,:,1,1), H(:,:,2,2), H(:,:,3,3), ...
52                   H(:,:,2,3) + H(:,:,3,2), ...
53                   H(:,:,1,3) + H(:,:,3,1), ...
54                   H(:,:,1,2) + H(:,:,2,1));
55     % Integrate local stiffness matrix with midpoint quadrature rule
56     Integrand = sum(Hessian .* permute(Hessian, [1 2 4 3]), [1 2]);
57     A4e(:,:,e) = area4e(e) * squeeze(Integrand);
58     % Integrate right-hand side by edge-oriented midpoint quadrature
59     b4e(:,e) = [zeros(1, 3), area4e(e) / 3 * valF4e(j,:)]';
60     % Evaluate derivatives of quadratic shape functions
61     Hess4e(:,:,e) = permute(Hessian, [3 1 2]);
62     Gradient = cat(3, [3 -1 -1 -1 1 1] .* GradP1(1,:)', ...
63                   [-1 3 -1 1 -1 1] .* GradP1(2,:)', ...
64                   [-1 -1 3 1 1 -1] .* GradP1(3,:)', ...
65                   [0 0 4 2 2 0] .* GradP1(2,:)', ...
66                   + [0 4 0 2 0 2] .* GradP1(3,:)', ...
67                   [0 0 4 2 2 0] .* GradP1(1,:)', ...
68                   + [4 0 0 0 2 2] .* GradP1(3,:)', ...
69                   [0 4 0 2 0 2] .* GradP1(1,:)', ...
70                   + [4 0 0 0 2 2] .* GradP1(2,:)'');
71     Grad4e(:,:,e) = permute(Gradient, [3 1 2]);
72 end
73
74 % COMPUTATION OF EDGE-ORIENTED LOCAL CONTRIBUTIONS
75 % Select gradients and Hessian of S2 basis functions for T+ and T-
76 % 1st to 3rd dimension : identical to Grad4e resp. Hess4e
77 % 4th dimension : 1 for T+ and 2 for T-
78 % 5th dimension : each edge
79 Grad4s = zeros(6, 2, 6, 2, nSides);
80 Grad4s(:,:,1,:) = Grad4e(:,:,e4s(:,1));
81 Grad4s(:,:,2,isInteriorSide) = Grad4e(:,:,e4s(isInteriorSide,2));
82 Hess4s = zeros(6, 2, 2, 2, nSides);
83 Hess4s(:,:,1,:) = Hess4e(:,:,e4s(:,1));
84 Hess4s(:,:,2,isInteriorSide) = Hess4e(:,:,e4s(isInteriorSide,2));
85 % Automatic choice of geometric penalty parameter
86 sigma4s = 3 * a * (length4s.^2) ./ area4e(e4s(:,1));
87 sigma4s(isInteriorSide) = sigma4s(isInteriorSide) / 4 ...
88   + 3/4 * a * length4s(isInteriorSide).^2 ...
89   ./ area4e(e4s(isInteriorSide,2));
90 % Local contributions to the jump term
91 J4s = zeros(9, 9, nSides);
92 % Local contributions to the penalty term
93 C4s = zeros(9, 9, nSides);
94
95 parfor s = 1:nSides
96     % Abbreviate local indices
97     Ind = localInd4s(:,:,s);
98     % Compute normal component of gradients
99     GradNormal = squeeze(sum(Grad4s(:,:,:,s) .* normal4s(s,:), 2));
100    % Jump of normal derivatives in the Simpson quadrature nodes
101    JumpNormal = [GradNormal(Ind(1:3,1),Ind(1:3,1),1) ...
102                - GradNormal(Ind(3:-1:1,2),Ind(3:-1:1,2),2); ...
103                GradNormal(Ind(4:6,1),Ind(1:3,1),1); ...
104                - GradNormal(Ind(4:6,2),Ind(3:-1:1,2),2)];
105    % Integrate penalty term by Simpson rule
106    Integrand = JumpNormal .* permute(JumpNormal, [3 2 1]);
107    C4s(:,:,s) = sigma4s(s) / 6 * squeeze(sum([1 4 1] .* Integrand, 2));
108    % Compute normal component of Hessian
109    HessNormal = squeeze(sum(Hess4s(:,:,:,s) .* normal4s(s,:), 2));
110    % Averages of the normal component of Hessian

```

```

92     MeanHessNormal = ...
93         [HessNormal(Ind(1:3,1),:,1) + HessNormal(Ind(3:-1:1,2),:,2);...
94           HessNormal(Ind(4:6,1),:,1); HessNormal(Ind(4:6,2),:,2)];
95     if isInteriorSide(s); MeanHessNormal = MeanHessNormal / 2; end
96     % Jump of gradient in the midpoint of the edge
97     JumpGrad = JumpNormal(:,2) * normal4s(s,:);
98     % Integrate jump term by midpoint rule
99     J4s(:, :, s) = length4s(s) * (MeanHessNormal * JumpGrad');
100 end

%% ASSEMBLING
% Indices for assembling of triangle-oriented contributions
101 RowIndices4e = permute(repmat(dof4e, [1 1 size(dof4e, 2)]), [1 3 2]);
102 ColIndices4e = permute(RowIndices4e, [2 1 3]);
% Indices for assembling of edge-oriented contributions
103 RowIndices4s = permute(repmat(dof4s, [1 1 size(dof4s, 2)]), [1 3 2]);
104 ColIndices4s = permute(RowIndices4s, [2 1 3]);
% Assembly of the system matrix and right-hand side
105 N = nNodes + nSides;
106 A = sparse(RowIndices4e(:), ColIndices4e(:), A4e(:), N, N);
107 J = sparse(RowIndices4s(:), ColIndices4s(:), J4s(:), N, N);
108 C = sparse(RowIndices4s(:), ColIndices4s(:), C4s(:), N, N);
109 B = A - J - J' + C;
110 b = accumarray(dof4e(:), b4e(:), [N 1]);

%% SOLUTION
% Determine degrees of freedom
111 n4sCb = n4s(~isInteriorSide,:);
112 CbNodes = unique(n4sCb(:));
113 [~, CbSides] = ismember(sort(n4sCb, 2), sort(n4s, 2), 'rows');
114 dof = setdiff(1:N, [CbNodes, nNodes + CbSides]);
115 ndof = size(dof, 2);
% Solution of algebraic system
116 u = zeros(N, 1);
117 u(dof) = B(dof,dof) \ b(dof);
118 end

```

Appendix B. A posteriori error estimation. The estimator $\eta^2(\mathcal{T}) := \sum_{T \in \mathcal{T}} \eta^2(T)$ with, for all $T \in \mathcal{T}$,

$$\begin{aligned}
 \eta^2(T) &:= \|h_T^2 f\|_{L^2(T)}^2 + \sum_{E \in \mathcal{E}(T)} \frac{\sigma_{\text{IP},E}^2}{h_E} \|[\nabla u_{\text{IP}}]_E \cdot \nu_E\|_{L^2(E)}^2 \\
 &+ \sum_{E \in \mathcal{E}(T) \cap \mathcal{E}(\Omega)} h_E \|[\partial_{\nu_E}^2 u_{\text{IP}}]_E\|_{L^2(\Omega)}^2
 \end{aligned}
 \tag{B.1}$$

from [8, Section 7.1] can be evaluated using some of the data structures from the previous appendix Section A.

```

1 vol4e = (area4e.^3) .* sum(valF4e.^2, 2) / 3;
2 u4e = u(dof4e');
3 u4s = u(dof4s');
4 penalty4s = sigma4s .* squeeze(sum(C4s .* permute(u4s, [2 3 1]) ...
5     .* permute(u4s, [3 2 1]), [1 2]));
6 tangents4e = (c4e(:, [3 1 2], :) - c4e(:, [2 3 1], :)) ...
7     ./ permute(length4s(s4e), [3 2 1]);
8 normal4e = [tangents4e(2, :, :); - tangents4e(1, :, :)];
9 signedNormal4e = ...
10 permute(reshape(normal4s(s4e(:), :), [nElem 3 2]), [3 2 1]);

```

```
11 HessU4e = squeeze(sum(Hess4e .* permute(u4e, [2 3 4 1]), 1));
12 BinormalU4e = ...
13     sum(permute(normal4e, [1 4 3 2]) .* HessU4e ...
14         .* permute(signedNormal4e, [4 1 3 2]), [1 2]);
15 jump4s = accumarray(s4e(:), biNormalU4e(:), [nSides 1]);
16 jump4s = (length4s).^2 .* jump4s.^2;
17 jump4s(CbSides) = 0;
18 eta4e = vol4e + sum(jump4s(s4e), 2) + sum(penalty4s(s4e), 2);
```

Appendix C. Downloads. The MATLAB function C0IP.m is available online and can be downloaded from the URL https://www.math.hu-berlin.de/~cc/cc_homepage/software/code/2022-PB_CC_JS-Parameter_free_C0IP/C0IP.m